C.L. Bottasso, F. Campagnolo, A. Croce, S. Dilli, F. Gualdoni, M.B. Nielsen
Structural Optimization of Wind Turbine Rotor Blades by Multilevel Sectional/Multibody/3D-FEM Analysis
Multibody System Dynamics, Vol. 32, N. 1, 2014, p. 87-116
doi:10.1007/s11044-013-9394-3

Multibody System Dynamics manuscript No.
(will be inserted by the editor)

Structural optimization of wind turbine rotor blades by multi-level sectional/multibody/3D-FEM analysis

C.L. Bottasso · F. Campagnolo · A. Croce · S. Dilli · F. Gualdoni · M.B. Nielsen

Received: date / Accepted: date

Abstract The present work describes a method for the structural optimization of wind turbine rotor blades for given prescribed aerodynamic shape. The proposed approach operates at various description levels producing cost-minimizing solutions that satisfy desired design constraints at the finest modeling level. At first, a "coarse"-level constrained design optimization is performed by using a 1D spatial geometrically exact beam model for aero-servo-elastic multibody analysis and load calculation, integrated with a 2D FEM cross sectional model for stress/strain analysis and the evaluation of the 1D model fully-populated cross sectional stiffness matrices. Next, a "fine"-level 3D FEM model is used for the refinement of the coarse-level solution. Improved results obtained at the level of the 3D model are utilized at the following coarse-level iteration through a heuristic modification of the design constraints. In addition, a buckling analysis is performed at the fine description level, which in turn affects the non-structural blade mass. The updated constraint bounds and mass make their effects felt at the next coarse-level constrained design optimization, thereby closing the loop between the coarse and fine description levels. The multi-level optimization procedure is implemented in a computer program and it is demonstrated on the design of a multi-MW horizontal axis wind turbine rotor blade.

Keywords Wind turbine · Blade design · Multibody dynamics · CAD modeling · FE analysis · Aero-servo-elasticity · Multi-disciplinary optimization

Paper submitted to *Multibody System Dynamics*, under review, 2012.

C.L. Bottasso
Wind Energy Institute, Technische Universität München, D-85748 Garching b. München, Germany, and
Dipartimento di Scienze e Tecnologie Aerospaziali, Politecnico di Milano, I-20156 Milano, Italy.
E-mail: carlo.bottasso@tum.de

F. Campagnolo · A. Croce · S. Dilli · F. Gualdoni
Dipartimento di Scienze e Tecnologie Aerospaziali, Politecnico di Milano, I-20156 Milano, Italy.

M.B. Nielsen
Department of Mechanical Engineering, Technical University of Denmark, DK-2800 Kgs. Lyngby, Denmark.

1 Introduction

The aero-structural design problem of wind turbine rotor blades concerns the definition of the optimal external aerodynamic shape and of the structural components of the blade that realize some desirable compromise among several figures of merit, including aerodynamic efficiency, weight, manufacturing costs, transportability, etc. All necessary trade-offs are usually considered and ultimately finalized within the more general problem of designing the whole wind turbine, where the goal is typically the minimization of the cost of energy.

This paper is concerned with the structural design of wind turbine rotor blades for given aerodynamic shape. Although this is only one aspect of the more general problem of designing a blade and a wind turbine, as mentioned above, it is nevertheless a highly complex and challenging task. In fact, the design should identify optimal structural layout, choice of materials and proper sizing of all structural members to ensure a cost-effective, safe and efficient operation throughout the lifetime of the machine. Given layout and materials, the sizing problem should be performed in such a way that all blade components (from webs, skin and spar caps, to root bolting and all the way down to glued connections, reinforcements, etc.) can withstand extreme loads and the effects of fatigue due to deterministic cyclic and stochastic turbulent excitations. Furthermore, the blade should be designed in such a way to avoid resonant conditions, which would increase vibrations and fatigue, be stiff enough to avoid striking the tower even under extreme operating conditions, be flutter-free in all of its operating envelope including emergency conditions, and also free from local instabilities such as skin buckling, wrinkling, etc. The design should also be able to fully exploit the anisotropic properties of composite materials, for example for inducing load mitigating couplings between blade bending and twisting [1]. Clearly, these goals should be met with the minimum possible cost, while satisfying all necessary manufacturing constraints.

The main challenge of this design problem comes from the need to marry the unsteady nature of loading in a wind turbine, which requires transient analyses, with the need to capture local effects such as stress concentrations and instabilities in complex 3D structures made with anisotropic composite materials. Transient analyses are routinely performed with beam-like models of the machine dynamics, coupled to suitable aerodynamic models and control laws that enable the simulation of the whole spectrum of unsteady operating conditions defining extreme loads and deflections, as well as fatigue. On the other hand, the verification of the local state of stress and strain and its stability are typically conducted with detailed 3D static finite element models, under loading conditions obtained from the ones computed with the transient models.

This two-stage analysis is typically performed “by hand”: after a first coarse-level preliminary sizing performed using beam-like models, one performs a fine-level verification using 3D FEM and corrects any possible deficiency, for example by increasing the thickness or lamination sequence of a component. Possibly, the result of the fine-level verification is used to update the coarse-level dynamic model and the process is iterated until convergence. Clearly, this procedure is time consuming and labor intensive. Furthermore, the design is not conducted as an integrated multi-level optimization, and might lead to sub-optimal results since there is not a consistent way to reflect the results of the fine-level analysis into modifications of the coarse-level models.

The scope of the present paper is to improve on the current design method of rotor blades, by proposing a multi-level design procedure that conducts the design in a fully integrated and automated manner. The method includes 2D finite element models for the characterization and analysis of the blade cross sections, aero-servo-elastic multibody models for load calculation according to certification guidelines [2,3], and detailed 3D finite element

models for detailed stress-strain, fatigue and buckling analysis. The design optimization is conducted by iterating among the various levels, so as to deliver a cost-minimizing design solution that also satisfies all desired design constraints at the finest description level, i.e. the detailed 3D model.

The design of wind turbine blades has been the subject of several investigations, and software packages are available that can support the process at the various necessary description levels. In the following we review some of the relevant literature, first for preliminary coarse-level sizing and then for detailed fine-level verification, and we compare the state-of-the-art with the new integrated and multi-level procedures proposed here.

As previously stated, a coarse beam model is often sufficient for preliminary analysis as it is capable of providing fast and accurate results for primary parameters such as natural frequencies, deflections, loads and the estimation of the overall dynamic behavior of the machine. At this stage, multibody procedures are routinely adopted, using geometrically exact beam formulations as in [4] and as in the non-linear finite-element-based multibody dynamics wind turbine simulation code `Cp-Lambda` (Code for Performance, Loads, Aero-Elasticity by Multi-Body Dynamic Analysis) [5,6] used here, or with Timoschenko beam elements as in [7]; modal representations of the flexible elements are also in widespread use, as in the wind turbine aero-elastic codes `FAST` [8] and `GH-Bladed` [9].

The use of such tools for preliminary design of rotor blades has been described in a few publications. In particular, the codes `RotorOpt` [10,11] and `FOCUS6` [12] implement integrated design environments. A suite of design tools is described in [13], providing the facilities for preliminary blade design, although the various software modules do not appear to be integrated in a unified optimization framework. Recently, the multi-disciplinary wind turbine design code `Cp-Max` (Code for Performance Maximization) was described in [14]. In that work, the structural blade design problem is formulated as a constrained optimization based on a two-level modeling system. The first level is represented by a parametric aero-servo-elastic multibody model, while the second level by 2D finite element parametric models of the blade cross sections. The integration of the two models allows for the synthesis of a beam given its cross sections, and for the evaluation of the sectional loading given the beam one, which are the two crucial steps of the design problem. In fact, from the sectional models, fully-populated stiffness matrices are computed using the code `ANBA` (Anisotropic Beam Analysis), based on the anisotropic beam theory formulated in [21]. The stiffness matrices obtained in this way are used for defining geometrically exact shear and torsion-deformable beams [19] in `Cp-Lambda`. On the other hand, recovery relations provided by `ANBA` allow for the computation of local sectional stresses and strains based on internal stress resultants computed with `Cp-Lambda`.

The formulation described in [14] enables the structural optimization of rotor blades through the integration of 2D cross sectional analysis and 1D spatial beam models. Although that paper mentioned the link towards a detailed fine-level 3D FEM verification of the design, the formulation lacked the ability to close the loop from fine-level analysis back to coarse-level representation, which is the only way one can generate a design that is optimal and constraint satisfying at the finest description level. This loop closure capability is described in the present work, and has been incorporated in an updated version of the `Cp-Max` software.

Several tools have been developed for the detailed structural analysis of wind turbine blades, typically developed in the form of pre- and post-processing software interfaced with commercial FE solvers. For example, `NUMAD` [15] serves as a pre-processor for the commercial FE software `ANSYS`. Given an externally generated CAD model, the code produces a mid-thickness model of the blade, meshes it using shell elements, and lets the user define all

necessary material properties, loading and boundary conditions for the required analyses. Similarly, FOCUS6 is also capable of generating detailed structural models of rotor blades using lay-up shell elements, while NSE-blade-mesher [16] exploits a combined solid and shell element mesh in connection with the FE solver ABAQUS. This code was used for confirming the bending and twisting behavior of a blade predicted by sectional analysis in [17], while a full structural multi-criteria optimization for a given aerodynamic shape is performed in [18] by utilizing a parametric FE model using ANSYS.

Here, a new tool is described for the automatic generation and analysis of 3D FE structural blade models. First, a detailed CAD model is generated in terms of NURBS (Non-Uniform Rational B-Splines) surfaces directly from the blade geometry obtained at the coarse description level. Next, the CAD model is associated with material properties, boundary as well as extreme and fatigue loading conditions, and meshed into shell or solid elements to enable the execution of the necessary analyses.

Static deflection and fatigue analyses are conducted on the fine-level 3D model, with the goal of verifying the satisfaction of the stress, strain and fatigue constraints, since the 3D model can represent effects that sectional and beam models cannot capture. Furthermore, a non-linear buckling analysis is performed under the maximum tip deflection loads.

A heuristic approach is used for incorporating the effects of the 3D FEM level analyses back into the coarse-level model. This way, new 2D sectional models are generated which in turn define a new 1D spatial beam model, and the complete process is repeated. Typically, very few iterations between the coarse and fine levels are necessary for convergence.

Through the new procedure described herein, a multi-level optimization is used to determine cost-minimizing design solutions that satisfy all desired constraints at the finest description level within reasonable computational costs. In particular, the loop closure between fine 3D FEM static and coarse multibody dynamic and cross sectional models is the main contribution of the present paper, and it has not been described before to the authors' knowledge.

The paper is organized as follows. At first, the general principles of the multi-level optimization procedure are described in §2.1 and the algorithmic organization of the code is illustrated in §2.2. Next, a detailed description is given in Sect. 3 of the various tasks that implement the automated CAD and FE model generation procedures and associated FE analyses, starting with a brief discussion of the relevant modeling aspects in §3.1. The description of the CAD model generation of the various components of the blade follows in §3.2, and the generation of the FE model is given in §3.3. This modeling task is conducted in two different manners tailored to the subsequent meshing, as described in §3.3.1, which is performed using either layered composite shells or solid elements. The correct orientation of the anisotropic material properties is addressed in §3.3.2, while the conversion of the relevant envelope load cases from the coarse description level into representative loading conditions for the 3D FE model is described in §3.3.3. Finally, the fine-level analyses are discussed in §3.4. The paper is complemented by Sect. 4, where the capabilities of the proposed integrated multi-level optimization procedures are illustrated on the structural design of a blade for a 2MW horizontal axis wind turbine.

2 Multi-level structural optimization of wind turbine rotor blades

2.1 Overview of multi-level optimization

Figure 1 illustrates the proposed multi-level constrained structural design optimization of wind turbine rotor blades, which is briefly described here below.

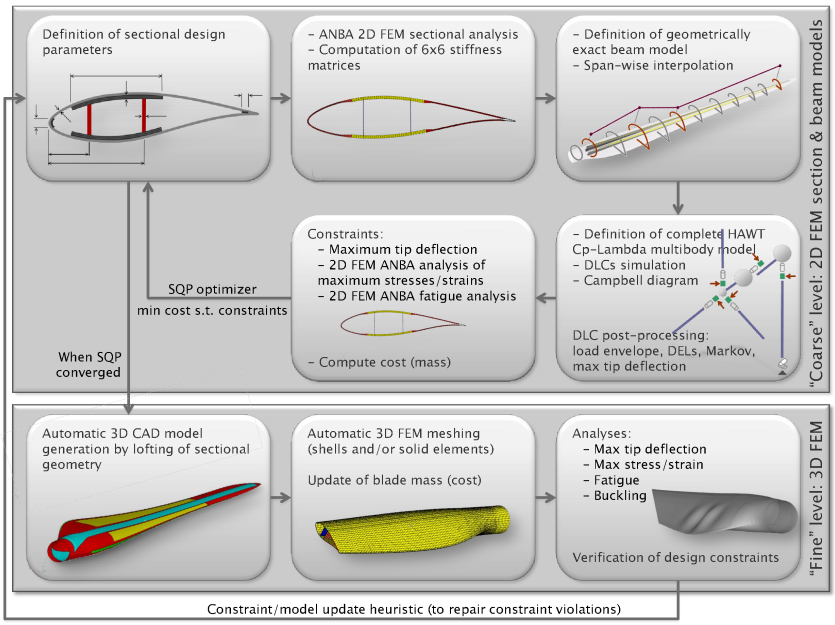

Figure 1 Multi-level structural blade optimization for given aerodynamic shape

As a starting point for the optimization, an initial definition of the blade structural configuration and associated material properties is required. Next, the primary design variables are defined at selected span-wise sections, typically including the thicknesses of skin, shear webs and spar caps as well as the area of the leading and trailing edge reinforcements; intermediate values along the blade span are interpolated using shape functions.

Based on this and all other necessary input data, a complete aero-servo-elastic model of the machine is developed using the wind turbine simulation code `Cp-Lambda`. All entities in the model are described using Cartesian coordinates in a single inertial frame, and constraints are enforced using Lagrange multipliers. Blades are described using a geometrically exact shear and torsion deformable beam model [19], which can represent arbitrarily large three dimensional rotations and displacements; spatial discretization is obtained using an iso-parametric formulation, resulting in a non-linear full finite element method. Time integration of the resulting differential algebraic multibody equations of motion in index-3 form is performed using a non-linearly unconditionally stable energy decaying integration scheme [20]. The code supports static and transient analyses as well as the computation of frequencies and mode shapes about deformed equilibrium configurations.

Each blade is described in terms of cross sectional properties computed at user-selected span-wise stations; for the computation of transient loads the number of sections is of the or-

der of one-hundred, while in the optimization loop defining the blade properties a few tens of sections are usually sufficient. Sectional stiffness matrices accounting for all possible structural couplings are computed using the code ANBA [21], based on either 2D finite element meshes or equivalent panels. In the latter case, which is the one considered here, each section is meshed with a number of panels ranging between one-hundred and one-hundred and fifty, depending on the local geometry. Each blade is finally modeled as a geometrically exact beam, using a number of cubic elements between twenty and thirty.

The aerodynamic loads computation is based on classical Blade Element Momentum (BEM) theory. Blades are associated to lifting lines described by three-dimensional twisted curves, and aerodynamic loads are then computed on the basis of local flow characteristics and local airfoil aerodynamic coefficients, stored in look-up tables [14].

The topological description of the wind turbine multibody model is reported in Fig. 2. The turbine flexible bodies — i.e. the blades, tower and drive train — are modeled by beam elements, while rigid bodies are used to model the inertial properties of the hub, generator and nacelle. Revolute joints are used for the pitch and rotor degrees of freedom, and are connected to the outputs of their relevant actuator models, while the tower foundation characteristics are modelled with torsional springs and dampers.

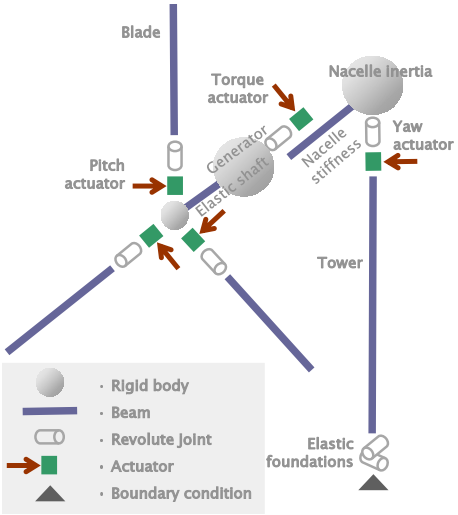

Figure 2 Topological representation of wind turbine multibody model

The model is supplemented by a regulation strategy and a collective-pitch/torque controller based on a speed-scheduled linear quadratic regulator (LQR) [22], capable of controlling the machine over its entire operating envelope.

With the closed-loop aero-servo-elastic model, transient design load cases (DLCs) are simulated that include turbulent wind cases, extreme gusts and a variety of fault conditions, according to [2,3]. Automatic procedures manage the post-processing of all generated results, to define a generalized load envelope. Sectional load envelopes are extracted as matrices containing values of the maximum and minimum internal stress resultants. In the present work, a generalized load envelope is defined that also includes the time histories of turbulent loads due to DLC 1.2 [2], used for the determination of fatigue damage, as well as the loads

associated with the maximum tip deflection. The determination of the latter loading condition is formulated as an optimization problem that looks for a set of equivalent static loads that, together with gravitational and inertial loads associated with the operational conditions at the time when the maximum tip deflection occurs, closely match the actual deflections and internal stress distribution [14].

Using the generalized load envelope, for each instantiation of the blade design one can compute all relevant design quantities, such as maximum tip deflection, stress and strain states at selected verification points in a number of span-wise sections through recovery relations provided by `ANBA`, and the level of fatigue-induced damage at the same verification spots. These quantities are then enforced as inequality constraint conditions for the optimization problem.

The code also computes the Campbell diagram of the machine, so that constraint conditions ensuring a resonant-free design can be included in the optimization. Furthermore, one can also include additional constraints on the unknown design parameters, such as bounds on the span-wise ply tapering rates or on the relative position between sectional center of gravity and pitch axis.

In this work, the merit function of the optimization problem is represented by the total mass of the blade. This quantity is computed based on the spatial and sectional configuration of the blade and also includes non-structural masses due to surface coating, foam core, resin take-up, etc. Here, it is implicitly assumed that mass is well-correlated with cost; the choice of mass as the merit function is also due to the fact that reliable cost models are not available in the public domain.

The constrained multi-disciplinary optimization is run until convergence using the sequential quadratic programming (SQP) method implemented in the `fmincon` routine of the `Matlab` software [23]. In order to reduce the computational cost, the optimization is run for a frozen load envelope; once the cost optimization converges, a new aero-servo-elastic wind turbine model is generated following the previously described steps and the relevant analyses are repeated for updating the generalized load envelope. The optimization is repeated until no more changes in the load envelope and the design are detected, which typically takes very few iterations. This procedure minimizes the number of evaluations of the generalized load envelope so as to reduce the computational cost [14].

From the computed blade geometry the code automatically generates a 3D CAD model, which precisely accounts for all components of the blade (shear webs, web core, flanges, spar caps, leading and trailing edge reinforcement, internal skin, skin core and external skin) as well as their associated material properties and laminate characteristics (see Sect. 3). The meshing of the blade is performed with the commercial pre-processing software `HyperMesh` [24], which provides macro-based facilities for automatic mesh generation using either shell or solid elements and the subsequent export of the model data in the form of input files compatible with various commercial FE solvers.

The 3D FE model provides the framework for a fine-level verification of the design constraint inequalities associated with admissible stresses, strains, deflections and fatigue damage, as the detailed model reveals effects that may have been overlooked by the coarse quasi-3D model composed of 1D spatial beam and 2D cross sectional models. For example, local stress concentrations at the beginning and end of the spar caps or at regions with rapidly changing geometry in the span-wise direction cannot be correctly represented by beam models, since in these cases the very hypotheses underlying beam theories are violated. In case constraint violations are detected at the fine-level, the coarse optimization loop is repeated with constraint bounds that are tightened proportionally to the violation

amount; coarse and fine-level iterations are repeated until an optimal design that satisfies the constraint conditions at the finest description level is obtained.

In addition, the 3D model can be used for designing secondary structural components, as for example the thickness of the skin core through a linearized buckling analysis. This in turn affects the non-structural mass of the blade model leading to an improved estimate for the cost function. This mass change affects the coarse-level analysis, that is then repeated until convergence; this is usually accomplished in a few iterations as illustrated in §4.3.

2.2 Algorithmic organization of multi-level optimization

The multi-level optimization for minimum blade weight that was sketched in the previous pages, can be more precisely expressed in the following algorithmic form:

$$\textbf{Function } (\boldsymbol{p}_s^*, w^*) = \texttt{MinBladeWeight}(\boldsymbol{p}_a, \boldsymbol{p}_s, D, \Gamma_s) : \tag{1a}$$
$$(\boldsymbol{E}) = \texttt{LoadEnvelope}(\boldsymbol{p}_a, \boldsymbol{p}_s, D), \tag{1b}$$
$$\textbf{do} \tag{1c}$$
$$(\boldsymbol{p}_{s1}, \boldsymbol{p}_{s2}) = \boldsymbol{p}_s, \tag{1d}$$
$$(\boldsymbol{p}_{s1}^*, w_1^*) = \texttt{MinWeightBladeFrozenLoads}(\boldsymbol{p}_a, \boldsymbol{p}_{s1}, D, \boldsymbol{E}, \Gamma_s), \tag{1e}$$
$$(M) = \texttt{3DCADAndFEMeshGeneration}(\boldsymbol{p}_a, \boldsymbol{p}_{s1}^* \cup \boldsymbol{p}_{s2}, \boldsymbol{E}), \tag{1f}$$
$$(\boldsymbol{p}_{s2}^*, w_2^*, \Gamma_s') = \texttt{3DFEAnalysis}(M, \boldsymbol{p}_{s2}, D, \boldsymbol{E}, \Gamma_s), \tag{1g}$$
$$\boldsymbol{p}_s^* = \boldsymbol{p}_{s1}^* \cup \boldsymbol{p}_{s2}^*, \tag{1h}$$
$$(\boldsymbol{E}') = \texttt{LoadEnvelope}(\boldsymbol{p}_a, \boldsymbol{p}_s^*, D), \tag{1i}$$
$$\Delta p_{s1} = \|\boldsymbol{p}_{s1}^* - \boldsymbol{p}_{s1}\|, \quad \Delta \boldsymbol{E} = \left\|\boldsymbol{E}' - \boldsymbol{E}\right\|, \tag{1j}$$
$$\boldsymbol{p}_s = \boldsymbol{p}_s^*, \quad \boldsymbol{E} = \boldsymbol{E}', \quad \Gamma_s = \Gamma_s', \tag{1k}$$
$$\textbf{while } (\Delta p_{s1} \geq \mathrm{tol}_{p_{s1}} \textbf{ and } \Delta \boldsymbol{E} \geq \mathrm{tol}_E). \tag{1l}$$

Here and in the following, functions are indicated with the notation

$$(O) = \texttt{FunctionName}(I), \tag{2}$$

where I indicates a list of input variables, while O a list of output ones.

In (1a), the mass optimization function takes as input the known and given parameters $\boldsymbol{p}_a$ describing the aerodynamic shape of the blade, the unknown structural parameters $\boldsymbol{p}_s$, the additional data structure D and list of constraint bounds Γ_s, and returns the optimal values of structural parameters $\boldsymbol{p}_s^*$ and corresponding blade weight w^*.

Unknowns $\boldsymbol{p}_s$ are partitioned into primary structural variables $\boldsymbol{p}_{s1}$, which are designed during the coarse optimization, and secondary structural variables $\boldsymbol{p}_{s2}$, such as the skin core thickness that can only be analyzed in the 3D FE model. List D contains all relevant data describing the characteristics of the machine

$$D = \left\{P_r, V_{\text{in}}, V_{\text{out}}, R, H, \text{AF}, C, v_{\text{tip}_{\max}}, L_{\text{DLC}}, \ldots\right\}, \tag{3}$$

which, among others, include rated power P_r, range between cut-in V_{in} and cut-out V_{out} wind speeds, rotor radius R, tower height H, list of airfoil data $\text{AF} = \{\ldots, \text{AF}_i, \ldots\}$, wind turbine class C [2], maximum admissible tip speed to limit noise emissions and list $L_{\text{DLC}} = \{\ldots, \text{DLC}\,i.j, \ldots\}$ containing all DLCs according to [2,3] used for blade sizing. Finally, Γ_s is

a vector of constraint parameters used for enforcing the design inequalities during structural optimization, defined as

$$\Gamma_s = \left(\boldsymbol{\sigma}_{\text{adm}}, \boldsymbol{\epsilon}_{\text{adm}}, \boldsymbol{\delta}_{\text{tip,max}}, [\omega_L, \omega_U], \ldots\right)^T, \tag{4}$$

where $\boldsymbol{\sigma}_{\text{adm}}$ and $\boldsymbol{\epsilon}_{\text{adm}}$ denote the admissible magnitudes for stress and strain components, $\boldsymbol{\delta}_{\text{tip,max}}$ is the maximum admissible tip deflection and the interval $[\omega_L, \omega_U]$ represents bounds for the placement of selected natural frequencies.

The coarse-level optimization for the primary structural design variables, $\boldsymbol{p}_{s1}$, is performed using the quasi-3D beam model in (1e), as illustrated by the "coarse" level block in Fig. 1. Next, the 3D CAD model is created and its mesh M is generated in (1f), as described later on in Sect. 3. Finally, the refined structural analysis in terms of the 3D FE model is performed in (1g), which yields updated values of the secondary design variables, $\boldsymbol{p}_{s2}$, and of the design inequality parameters, Γ_s. These three steps are shown in the "fine" level block of Fig. 1.

As pointed out in [14], the recalculation of the full load envelope $\boldsymbol{E}$ for each change in the structural design variables may imply a considerable computational cost. Therefore, the coarse (1e) and fine (1g) level steps are conducted considering the load envelope $\boldsymbol{E}$ as frozen. However, it should be emphasized that the effects of the design on the load envelope is recovered by the iteration in (1c–1l), so that the procedure has the sole effect of reducing the computational cost but does not affect the results.

The coarse-level constrained optimization (1e), which is solved using the SQP algorithm, takes the form

$$\textbf{Function } (\boldsymbol{p}_s^*, w^*) = \texttt{MinWeightBladeFrozenLoads}(\boldsymbol{p}_a, \boldsymbol{p}_s, D, \boldsymbol{E}): \tag{5a}$$

$$\boldsymbol{p}_s^* = \min_{\boldsymbol{p}_s} W(\boldsymbol{p}_s, D) \quad (\text{and } w^* = \arg\min_{\boldsymbol{p}_s} W), \tag{5b}$$

$$\text{s.t.:} \quad \boldsymbol{g}_s(\boldsymbol{p}_s) \leq \boldsymbol{0}, \tag{5c}$$

$$\boldsymbol{\omega}(\boldsymbol{p}_s, D) \in [\boldsymbol{\omega}_L, \boldsymbol{\omega}_U], \tag{5d}$$

$$\boldsymbol{\sigma}(\boldsymbol{p}_s, \boldsymbol{E}, D) \leq \boldsymbol{\sigma}_{\text{adm}}, \tag{5e}$$

$$\boldsymbol{\epsilon}(\boldsymbol{p}_s, \boldsymbol{E}, D) \leq \boldsymbol{\epsilon}_{\text{adm}}, \tag{5f}$$

$$\boldsymbol{d}(\boldsymbol{p}_s, \boldsymbol{E}, D) \leq 1, \tag{5g}$$

$$\boldsymbol{\delta}_{\text{tip}_{\text{max}}}(\boldsymbol{p}_s, \boldsymbol{E}, D) \leq \boldsymbol{\delta}_{\text{tip}_{\text{adm}}}. \tag{5h}$$

The design constraint inequalities for this problem involve the following conditions:

- (5c): requirements on the unknown structural parameters, such as for example limits on the span-wise ply tapering rates.
- (5d): the placement of significant natural frequencies to lie within a desired interval $[\omega_L, \omega_U]$ in order to avoid resonant conditions. This could be a requirement for the first flap-wise blade eigenfrequency to lie above the three-per-rev frequency at the rated rotor speed, or a requirement for a suitable gap between two consecutive blade frequencies.
- (5e,5f): bounds on stress and strain components $\boldsymbol{\sigma}$ and $\boldsymbol{\epsilon}$, respectively, at a selected number of points on cross sections of interest, in order so ensure sufficient structural strength according to [2,3].
- (5g): criterion on fatigue induced damage in turbulent wind conditions DLC 1.2 [2]. Damage d_{σ_r} at a point on a cross section due to a single stress component σ_r is computed according to [2], while a multi-axial damage index d is computed according to [25,26] as

$$d = d_{\sigma_1}^{2/m} + d_{\sigma_1}^{2/m} - (d_{\sigma_1} d_{\sigma_2})^{1/m}) + d_{\sigma_6}^{2/m}, \tag{6}$$

where m denotes the inverse slope of the S-N curve and indices 1, 2 and 6 refer to the longitudinal, transverse and shear stress components, respectively. The damage indices d for each verification point on each cross section are collected in a vector $\boldsymbol{d}$ and are all bounded to unity.

– (5h): a limit on the maximum blade tip deflection throughout all time histories of all DLCs.

The fine-level analysis (1g) can be stated in the following algorithmic form:

$$\textbf{Function } (\boldsymbol{p}^*_{s2}, w^*_2, \Gamma'_s) = \texttt{3DFEAnalysis}(M, \boldsymbol{p}_{s2}, D, \boldsymbol{E}, \Gamma_s): \tag{7a}$$

$$(\boldsymbol{p}^*_{s2}, w^*_2) = \texttt{MinSecondaryWeight}(M, D, \boldsymbol{E}), \tag{7b}$$

$$\Gamma'_s = \texttt{ConstraintVerificationAndUpdate}(M, D, \boldsymbol{E}, \Gamma_s), \tag{7c}$$

and comprises of two main steps.

The first, (7b), concerns the design of secondary structural parameters, in this case represented by the skin core thickness with respect to local buckling. This problem yields the optimal values of the secondary variables $\boldsymbol{p}^*_{s2}$, as well as an improved estimate for the blade mass $w^* = w^*_1 + w^*_2$. The buckling analysis in itself can be formulated as the following constrained optimization:

$$\textbf{Function } (\boldsymbol{p}^*_{s2}, w^*_2) = \texttt{MinSecondaryWeight}(M, D, \boldsymbol{E}): \tag{8a}$$

$$\boldsymbol{p}^*_{s2} = \min_{\boldsymbol{p}_{s2}} W_2(M, D) \quad (\text{and } \; w^*_2 = \arg\min_{\boldsymbol{p}_{s2}} W_2), \tag{8b}$$

$$\text{s.t.:} \quad \boldsymbol{\lambda}(M, D, \boldsymbol{E}) \geq 1, \tag{8c}$$

where $\boldsymbol{\lambda}$ are the eigenvalues of the linearized buckling problem associated with the loading conditions stored in the generalized envelope $\boldsymbol{E}$. Further details on the solution of this problem are given in §3.4.4.

The second step, (7c), concerns the verification of the design constraint conditions on the 3D FE model through static, modal and fatigue analyses. If constraint violations are detected, updated constraint bounds Γ'_s are generated, that will in turn affect the next solution of problem (1e). The design constraint that are verified at this level are:

– Placement of natural frequencies, corresponding to the coarse-level inequalities (5d).
– Bounds on stress and strain components, corresponding to the coarse-level inequalities (5e,5f).
– Fatigue induced damage constraints, corresponding to the coarse-level inequalities (5g).
– Maximum blade tip deflection, corresponding to the coarse-level inequality (5h).

If the verification of the constraint conditions on the fine-level model performed in (7c) reveals that some design inequalities are not satisfied, a heuristic approach is applied in which the constraints are modified proportionally to the violation amount. Assume that a condition for maximum stress $\sigma_{\max,2D}$ is satisfied at a given section $\sigma_{\max,2D} < \sigma_{\text{adm}}$ at the end of the ith coarse-level optimization, but it is violated when the fine-level 3D analysis is performed, i.e. $\sigma_{\max,3D} > \sigma_{\text{adm}}$. Then the admissible stress for the $(i+1)$th iteration is modified as

$$\sigma^{(i+1)}_{\text{adm}} = s_\sigma \, \sigma^{(i)}_{\text{adm}}, \tag{9}$$

where $s_\sigma = \sigma_{\max,3D} / \sigma_{\max,2D}$. This way, a more stringent constraint condition is imposed at the next coarse-level iteration. It may be expected that the stress ratio between the quasi-3D and the 3D analyses is almost constant for moderate variations of the structural element sizes. Therefore, the present approach may be used for refining the coarse-level analysis

according to the results from the fine-level solution. The other constraint parameters Γ_s are handled in a similar way, so that the full set of constraint limits may be updated as

$$\Gamma_s' = \boldsymbol{S}\Gamma_s, \tag{10}$$

where $\boldsymbol{S}$ is a diagonal matrix containing the constraint limit modification factors $s_{(\cdot)}$ for each of the constraint conditions.

3 CAD modeling, FE generation and analysis

Crucial to the success of the present automated optimization procedure is the construction of a robust and reliable finite element model. For a complex structure such as a wind turbine blade this requires several steps, which can be summarized as:

- Parametric definition of each blade component, either in terms of its bounding surfaces or of the laminate mid-planes, as described in §3.2.
- Generation of a complete FE model, described in §3.3, which in turn requires:
  - Mesh generation, including both the 3D blade discretization using either shell or solid elements and the discretization of 2D cross sections for sectional analysis in terms of panel or surface elements, as described in §3.3.1.
  - Assignment of element properties, including the laminate ply stacking sequences and associated thicknesses, material parameters and fiber orientations, as detailed in §3.3.2.
  - Conversion of the 1D spatial beam model loading conditions into equivalent conditions for the 3D FE model, as described in §3.3.3.
- FE analysis and post-processing of the results for the verification of the relevant design conditions, as detailed in §3.4.

In this work, the CAD model generation, as well as the assignment of the associated material properties and loading conditions, is based on the information from the coarse-level optimizer, and it is performed in `Matlab`. The FE mesh generation is performed using the batch meshing facilities of `HyperMesh`, where the required scripts are generated in `Matlab`. Finally, `Matlab` scripts handle the batch submission of the various analyses performed using `MSC Nastran` [27], as well as their post-processing.

3.1 Modeling aspects

The way in which the FE modeling of wind turbine blades is conducted may have a significant influence on the procedures used for generating the CAD geometry. The most frequently used technique for blade modeling is based on layered shell elements [15, 12], which are commonly available in commercial FE solvers. Most implementations provide the possibility of specifying the extent of the elements in terms of offsets from a reference surface other than its mid-thickness. This is particularly convenient when dealing with wind turbine blades, as the elements can be specified with respect to the exterior surface defined by the shape of the airfoils. Since the external shape is smooth, the generation of the necessary CAD model is not particularly complicated.

However, a possible drawback of the offset technique is that it may result in the erroneous prediction of the torsional behavior of the blade [30]. This problem is of particular concern since torsion affects loading through changes in the angle of attack, as for example

explicitly exploited for load mitigation in bend-twist coupled rotor blades [1]. Recent improved shell formulations circumvent this problem, as for example element `SHELL281` [32] or the pre-integrated matrix input [33] available for `ANSYS`.

Otherwise, one can generate a mid-thickness CAD model of the blade, as done manually in [31]. The construction of the geometry using mid-thickness surfaces, illustrated in Fig. 3(a) at left, is in general rather cumbersome, since thickness variations lead to step changes between contiguous mid-thickness surfaces.

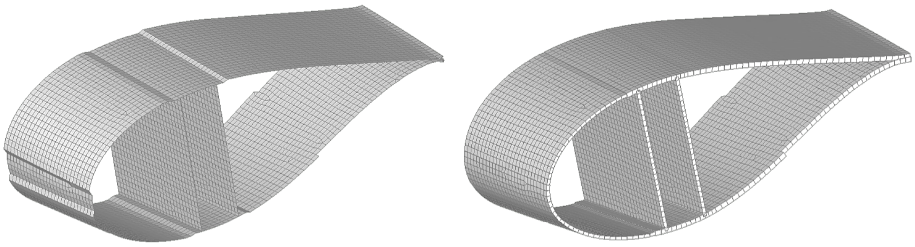

(a) Mid-thickness shell elements (b) Solid elements

Figure 3 Two possible FEM models of rotor blades

Alternatively, solid elements can be used for building the mesh, as shown in Fig. 3(b) at right. These are particular suitable for capturing inter-laminar stresses, for delamination and debonding analysis. However, the use of solid elements may complicate the CAD generation, since both the external and internal surfaces must be defined, which may be cumbersome to do in the various transition zones of a blade. Furthermore, one should pay specific attention to the accurate definition of the material property orientation [34]. While procedures for associating the correct material orientation to models composed of shell elements are rather well established (e.g. by direct projection of a user-defined material reference vector on the element [35]), the case of complex models composed of solid elements requires special attention as individual local coordinate systems must be defined for each element in the mesh.

For generality, the present implementation supports all approaches mentioned above, so that one may generate mid-thickness or exterior surface shells with offsets, or, alternatively, solid element meshes. It further includes 2D sectional meshing capabilities, based on either panel or 2D surface elements, to be used for sectional analysis in `ANBA`.

3.2 CAD model

The generation of a complete CAD surface model for shell meshing is accomplished as follows.

A number of cross sections, typically of the order of one hundred, are obtained by thickness-interpolation of the generating airfoil data points, using their span-wise chord and twist distributions. Chordwise spline interpolations are used for parameterizing the airfoils from their data points, and nodes define the location of the boundaries of the projections of the various blade elements (spar caps, shear webs, etc.) onto the external blade surface, as illustrated in Fig. 4(a).

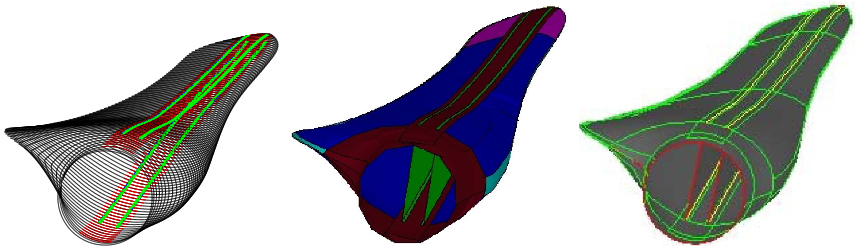

(a) Interpolation of airfoil data points

(b) NURBS surfaces

(c) Partitioning in simple sub-surfaces

Figure 4 Selected steps in the generation of the CAD model of a wind turbine blade

For mid-thickness CAD generation, an inward projection along the local normal is performed using the thickness information associated with each blade element. This way, steps at the boundaries between elements with different thicknesses are generated. The thickness data accounts for span-wise variations, as computed by the coarse-level optimization, as well as user-defined chord-wise variations; the latter ones are used to avoid modeling errors associated with the overlapping of inner skin/core, which are likely to occur near the trailing edge [17].

From the chordwise interpolations of the airfoils or their mid-thickness projections, collocation data points are obtained with sufficient sampling resolution (typically of the order of one thousand points per cross section) to allow for an accurate surface parameterization, which is obtained by using NURBS [36] on each surface describing a blade component projection. In the present implementation only non-rational surfaces are utilized, whose weights are equal to unity, and control points are obtained by least squares from collocation points. Collocation parameters for chord-wise interpolation are obtained using the centripetal method [37], while span-wise collocation parameters follow by averaging of the parameters determined at two consecutive sections. Once all collocation parameters are obtained, knot vectors are computed by using the average method suggested by de Boor [36]. An illustration of the resulting surface model is given in Fig. 4(b) for the case of mid-thickness representation.

For the construction of a solid mesh, the external blade surfaces are first generated as described above. Next, the various surfaces are further partitioned into simpler sub-surfaces, as illustrated in Fig. 4(c). Partitioning is performed such that, by extruding inwards each external sub-surface along the local thickness direction, one can obtain the associated facing internal sub-surface; this will allow for the generation of the solid mesh by means of a similar through-the-thickness extrusion of a surface mesh, as explained later on. Contact areas between two surfaces, as at the glued connections between shear webs and spar caps, are also used for the partitioning, so as to ensure conforming discretizations during meshing.

The information associated with the parametric NURBS representation of the resulting model is finally exported in IGES (Initial Graphics Exchange Specification) format towards `HyperMesh` for subsequent meshing.

The present approach, which tries to generate an accurate geometric model before meshing, differs significantly from the lofting of pre-defined cross sectional meshes used for example in [17], and presents several advantages. In fact, using this approach the shape of the internal skin as well as the transitions between zones with varying thickness along the span of the blade are precisely reconstructed. This is particularly important since these regions

must be accurately modeled [3], and it may be particularly useful in areas of rapid span-wise variations as the one between root and max chord span.

3.3 FE model

3.3.1 Mesh generation

The generation of an unstructured mostly quadrilateral shell mesh is obtained by using `HyperMesh` on the exterior or mid-thickness surface CAD model; a limited number of triangular elements is generally obtained close to corners and in a few difficult spots. The meshing algorithm ensures the conformity of the resulting grid across edges bounding the various sub-surfaces of the model.

An unstructured mostly hexahedral solid mesh is obtained by first quad meshing the external sub-surface of each individual blade component as for the shell case, projecting the mesh onto the opposite internal surface, optionally defining through-the-thickness discretizations by the same projection, and finally connecting the resulting surface grids into a solid one. Since the initial surface meshes are conforming, the final solid grid is also guaranteed to be conforming.

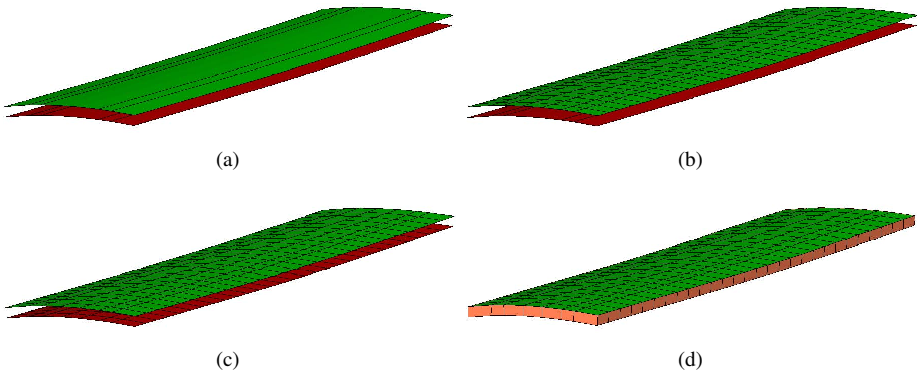

Figure 5 Surface meshing and extrusion procedure

The surface meshing and extrusion procedure is illustrated in Fig. 5 for a span-wise portion of the spar cap; notice that the external surface has been divided into several stripes in the chord-wise direction, to account for the glued connections with the shear webs. A span-wise portion of the resulting complete solid mesh is illustrated in Fig. 6(a), and details of the trailing edge with its reinforcement strip and the thickness variation of the core is shown in Fig. 6(b).

For sectional analysis, one can generate either a panel mesh, i.e. a discretization of the mid-thickness line in 1D elements, or a 2D mesh, i.e. a grid of quad or tria elements that discretize the various components of the cross section. The first option was used in the examples of the present paper, although the second is also implemented in the code and provides for a higher definition evaluation of the state of stress of the cross section, possibly including also the interlaminar stresses.

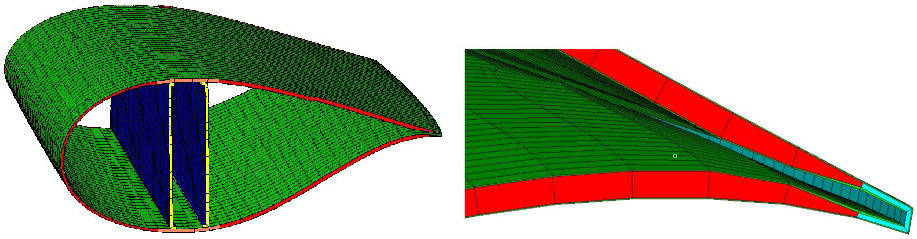

(a) (b)

Figure 6 Span-wise portion of solid mesh and trailing edge detail

For the panel case, meshing of the mid-thickness sectional line model is straightforward. For the 2D case, the external lines are first projected inwards by using the local normals, this way defining the bounding lines of the various blade component cross sections. The external line mesh is then extruded inwards, possibly realizing multiple through-the-thickness subdivisions, accounting for the local thickness information available at each cross section; connection of the external and extruded line meshes generates the cross sectional surface grid.

A 2D cross sectional mesh and a close-up view of the trailing edge area are illustrated in Fig 7(a) and 7(b), respectively.

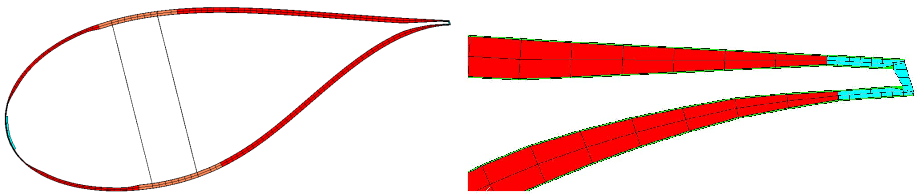

(a) (b)

Figure 7 2D mesh for cross sectional analysis

3.3.2 Material properties

Material properties, including the orientation of the fibers with respect to the pitch axis, are associated with the various entities of the CAD model during its definition.

Once the mesh has been generated, the definition of the material properties of each mesh element is obtained as follows. At first, the centroid of each element is computed; if the element is of the 3D type, its centroid is projected onto the master CAD face of that blade component. At that CAD face location, a local material reference frame is defined that has a unit vector in the direction of the fibers and a second unit vector along the local normal, computed from the NURBS surface parameterization. The orthotropic material properties of the element are then readily obtained by transforming into the local reference frame of that same element.

For shell meshes, the procedures support either the generation of single layer equivalent composite laminates or of layer-by-layer representations. The latter approach is particular

convenient for modeling very thin layers, such as the skin coating that would result in elements with very high aspect ratios. Even though such details of the blade design may seem to be of minor importance from the structural point of view, they can indeed have a significant influence on the estimation of the total mass (up to $4 \div 5\%$), with a consequent possible effect on the blade dynamic properties.

3.3.3 Equivalent loading conditions

In order to perform all relevant analyses on the fine-level FE model, appropriate loading and boundary conditions must be generated from the results of the coarse-level multibody simulations; these include loads inducing extreme stress and strain values, loads associated with maximum tip deflections, as well as time histories of the turbulent loads cases for the evaluation of fatigue damage. For each of these loading conditions, span-wise distributions of the internal stress resultants and of the aerodynamic forces are readily available from the multibody simulations. The computation of equivalent loading conditions for the FE model is here performed by distinguishing between aerodynamic and inertial loads. This way, realistic loading conditions for the blade can be established, e.g. by limiting the application of the aerodynamic loads to the external skin nodes.

Span-wise distributions of inertial loads are recovered by enforcing the equilibrium of a blade portion. With reference to Fig. 8, consider a blade segment $\eta \in [\eta_i, \eta_{i+1}]$, where $\eta \in [0,1]$ is the span-wise non-dimensional coordinate running along the beam reference line passing through the sectional point E. The internal stress resultants on the $(i+1)$th section is $\boldsymbol{f}_{i+1}$, and the moment resultant about E is $\boldsymbol{m}_{i+1}$, while the ones on the ith section negative face are $-\boldsymbol{f}_i$ and $-\boldsymbol{m}_i$, respectively. At the span-wise station η, per-unit-span aerodynamic forces $\boldsymbol{f}^A(\eta)$ and moments $\boldsymbol{m}^A(\eta)$ are applied at the aerodynamic reference line passing through the sectional point A, which is at a distance $\boldsymbol{r}^A(\eta)$ from point E on the ith section. Similarly, per-unit-span inertial forces $\boldsymbol{f}^I(\eta)$ and moments $\boldsymbol{m}^I(\eta)$ are applied at the beam reference line, which is at a distance $\boldsymbol{r}^I(\eta)$ from point E on the ith section.

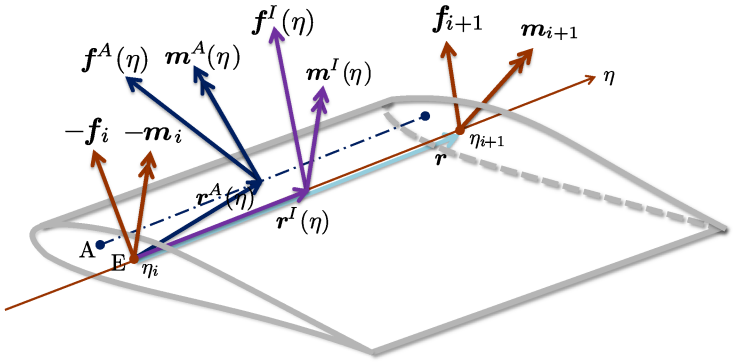

Figure 8 Recovery of inertial loads from sectional internal stress resultants and aerodynamic loads

The force and moment (about E) equilibrium conditions for the blade segment write

$$-\boldsymbol{f}_i + \boldsymbol{f}_{i+1} + \int_{\eta_i}^{\eta_{i+1}} (\boldsymbol{f}^A + \boldsymbol{f}^I)\,\mathrm{d}\eta = 0, \tag{11a}$$

$$-\boldsymbol{m}_i + \boldsymbol{m}_{i+1} + \int_{\eta_i}^{\eta_{i+1}} (\boldsymbol{m}^A + \boldsymbol{m}^I + \boldsymbol{r}^A \times \boldsymbol{f}^A + \boldsymbol{r}^I \times \boldsymbol{f}^I)\,\mathrm{d}\eta + \boldsymbol{r} \times \boldsymbol{f}_{i+1} = 0. \tag{11b}$$

By using a trapezoidal approximation for the span-wise integrals, one obtains

$$\int_{\eta_i}^{\eta_{i+1}} \boldsymbol{f}^I\,\mathrm{d}\eta \approx \frac{\eta_{i+1} - \eta_i}{2}(\boldsymbol{f}_i^I + \boldsymbol{f}_{i+1}^I), \tag{12}$$

where $\boldsymbol{f}_i^I$ and $\boldsymbol{f}_{i+1}^I$ are sectional inertial forces. By inserting (12) into (11a), starting from the blade tip, one may compute each sectional inertial force $\boldsymbol{f}_i^I$ based on the sectional resultants and aerodynamic loads. Similarly, from (11b) one may compute each sectional inertial moment $\boldsymbol{m}_i^I$.

Once sectional loads have been recovered as explained, they are applied to the blade structure by means of `RBE3` interpolation elements provided in the commercial FE solver `MSC Nastran` [27]. Different sets of nodes can be associated with different interpolation elements, each one in turn associated with a different set of forces and moments. This way aerodynamic loads can be applied to the sole skin nodes, while inertial loads can be applied to all sectional nodes; alternatively, combined loads can be applied to the spar cap nodes, as shown in Fig. 9. In all cases, forces are distributed to each node considering local user defined weighting factors, while moments are applied as sum of equilibrated forces on dependent nodes, as explained in [29]. An example of the application of loads to the spar cap of a shell 3D model is reported in Fig. 9.

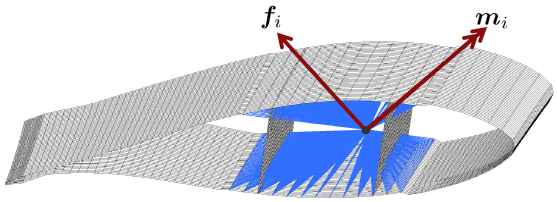

Figure 9 Load application to spar caps nodes using the `RBE3` element

A more realistic way of representing aerodynamic loads would be to reconstruct the chord-wise pressure distribution, for example using assumed shapes from experimental measurements or from suitable numerical models such as `Xfoil` [28]. This feature will be included in future releases of the code.

3.4 Analysis

The automatically generated 3D FE model enables the detailed fine-level verification of the various constraint inequalities associated with the overall optimization problem. Furthermore, it can be used for designing secondary structural parts such as the skin core thickness by means of a linearized buckling analysis. In the present section the assumptions and procedures for these various analyses are described.

3.4.1 Static analysis

Static analyses are performed for the verification of the constraint inequalities associated with the max/min allowable stresses/strains and the maximum tip deflection, with the aim of revealing possible effects not captured by the beam model.

For each user-defined verification section, the max/min stress/strain loading conditions are readily identified by scanning all DLCs of interest [14], and using the sectional recovery relations provided by `ANBA`. Next, the corresponding equivalent loading conditions are first computed as described in §3.3.3 from the coarse-level analysis, and then applied to the 3D FE model. Similarly, by scanning all DLCs, the maximum tip deflection condition is identified and translated into an equivalent loading condition.

Geometric and material linear static analyses are performed in `MSC Nastran`, and the relevant results in terms of strains, stresses and displacements are processed in `Matlab` to detect possible violations of the constraint conditions. It was verified that, for the examples developed in the present work, the use of geometrically non-linear analyses, as opposed to the present linear ones, yield only negligible differences, although this might not be the case for the future projected very long and slender next generation wind turbine blades.

3.4.2 Modal analysis

During coarse optimization, a design accommodating desired dynamic properties can be obtained by specifying suitable constraints for significant natural frequencies of the blade, as described in §2.2. Such constraints are typically expressed for the rotating blade at rated RPM. The inertial effects associated with blade rotation are taken into account in the `Cp-Lambda` modal analysis by first performing a non-linear static analysis subjected to a loading condition including the inertial effects of rotational motion, and then by performing a modal analysis about the resulting deformed configuration, accounting for the centrifugal stiffness term.

A similar procedure could be used for performing the modal analysis on the 3D FE model [27]. However, while coarse-level constraints are enforced for the rotating frequencies, the fine-level verification of the frequency conditions is performed here for simplicity as a standard non-rotating modal analysis about the blade undeformed configuration. In particular, ratios between corresponding non-rotating frequencies, computed on the coarse-level beam and fine-level FE models, are used as indicators of the disagreement between the two representations. This is a reasonable assumption, since both models are sophisticated enough to precisely account for inertia-related changes of frequencies, and thus the ratios between non-rotating frequencies are expected to change in a similar fashion. Furthermore, rotational effects on frequencies are typically rather limited for wind turbine rotor blades.

3.4.3 Fatigue analysis

Similarly to the coarse-level optimization procedure [14], the fine-level evaluation of damage caused by loads in turbulent wind conditions (DLC 1.2 [2]) is only conducted for a limited set of critical points at user-defined verification sections. Such critical points are identified during coarse optimization as the sectional spots where the multi-axial damage index d of Eq. (6) exceeds a specified threshold.

The stress time histories necessary for evaluating the damage index are conveniently computed by exploiting the linear superposition of static unit load cases applied to the FE model with load histories obtained from the beam model (see e.g. [38]). At each verification

point, a static force or moment (in the case of shells) of unit magnitude is applied, and the full stress time history follows as

$$\sigma_i(t) = \sum_j P_j(t) \frac{\sigma_{i,j}}{P_{j,\mathrm{FEA}}}, \tag{13}$$

where $P_j(t)$ denotes a load history obtained by a multibody transient simulation, $P_{j,\mathrm{FEA}}$ the applied unit load, and σ_i is the static stress resultant at point i for load case j. This procedure reduces the computational cost necessary for the evaluation of the full stress time history on the comprehensive 3D FE model. The remaining steps required for the computation of the damage index follow the same procedure used at the coarse analysis level, using rain-flow counting and the associated Markov matrices.

3.4.4 Buckling analysis

An additional feature only provided by a full 3D FE model is the capability of performing a linearized buckling analysis, which can be used for designing secondary structural elements, such as the skin and web core thicknesses. It is important to include the sizing of secondary components in the design process, because the distribution of the associated structural material has a significant influence on the non-structural mass, which in turn affects the dynamic behavior of the blade by changing its natural frequencies.

Prior to the FE analysis, an initial distribution of the core material and thickness for skin and webs can be estimated by the following two step procedure, based on simplified design formulas:

1. Choice of material. Appropriate stiffness properties for the core material are estimated such that local buckling (or wrinkling) is avoided, as this may cause fractures in the core or delamination. Following [39], this is accomplished by comparing the computed extreme compressive stress to the following critical stress:

$$\sigma_{\mathrm{adm,wrinkling}} = 0.5 \sqrt[3]{G_{\mathrm{core}} E_{\mathrm{core}} E_{\mathrm{skin}}}, \tag{14}$$

   where G and E denote the shear and Young's moduli, respectively.
2. Thickness sizing. For the skin and web panels, the critical buckling stress $\sigma_{\mathrm{adm,buck}}$ and shear $\tau_{\mathrm{adm,buck}}$ are computed using the following equations:

$$\sigma_{\mathrm{adm,buck}} = \frac{\pi^2}{t_{\mathrm{panel}} b^2} K_{\mathrm{c}} \sqrt{D_{11} D_{22}}, \tag{15a}$$

$$\tau_{\mathrm{adm,buck}} = \frac{\pi^2}{t_{\mathrm{panel}} b^2} K_{\mathrm{s}} \sqrt[4]{D_{11} D_{22}^3}, \tag{15b}$$

   where t_{panel} is the skin or web panel thickness, b is the panel edge width, D_{11} and D_{22} are the diagonal components of the out-of-plane bending stiffness matrix of the sandwich panels computed with classical laminate theory. Finally, K_{c} and K_{s} are buckling factors accounting for several properties of a sandwich structure, like its ortotrophy, curvature and out-of-plane shear flexibility, as well as for the way the longitudinal stress is distributed along the plate edge. For further details about the computation of the buckling factors see [41].

At several stations along the blade span, the skin core is sized by imposing the constraint $\lambda_s \geq 1$, where λ_s is the skin buckling load factor, computed by solving the following equation:

$$\lambda_s \left(\frac{\sigma}{\sigma_{\text{adm,buck}}} \right) + \lambda_s^2 \left(\frac{\tau}{\tau_{\text{adm,buck}}} \right)^2 = 1, \tag{16}$$

which takes into account stress-shear interactions [42]. Similarly, the web core is sized constraining $\lambda_w \geq 1$, where λ_w is the solution of:

$$\lambda_w^2 \left(\left(\frac{\sigma}{\sigma_{\text{adm,buck}}} \right)^2 + \left(\frac{\tau}{\tau_{\text{adm,buck}}} \right)^2 \right) = 1. \tag{17}$$

Subsequently in the design process, at the fine verification level and similarly to the case of the primary structural variables described in §2.2, the core thickness of a region where buckling occurs is increased by an amount proportional to the exceedance of the constraint condition $\lambda \leq 1$, where λ is the buckling eigenvalue associated with the applied load.

In the present implementation, the linear buckling analysis is performed using the loading condition that results in the maximum tip deflection of the blade, as this results in severe compressive loads on the suction side of the blade. Alternatively, loads associated with the extreme values of compressive stresses at relevant sections could be identified from the load envelope and used for the buckling analysis.

4 Applications and results

4.1 Baseline wind turbine

In this section the performance of the developed multi-level optimization procedures is illustrated with respect to a Class-IIIA 2MW HAWT with a 45 m rotor radius. The structural layout of the blade is a stressed-shell configuration with single upper and lower spar caps confined within two planar shear webs, normal to the maximum chord line. The primary structural design parameters $\boldsymbol{p}_{s1}$ are defined as the common thickness of the two shear webs, the common thickness of the upper and lower spar caps and the thickness of the external blade shell. These quantities are represented by span-wise linear interpolations of corresponding nodal unknowns located at η =0, 0.01, 0.03, 0.10, 0.195, 0.20, 0.25, 0.4, 0.5, 0.6, 0.75, 0.8, 0.98 and 1, resulting in a total number of primary structural design parameters equal to 53. A typical blade section is reported in Fig.10.

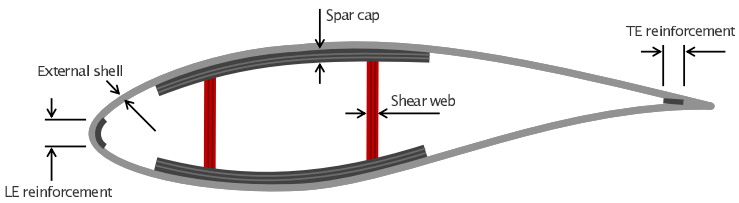

Figure 10 Primary structural design parameters on a typical section

The main blade structural components are reported in Table 1. The blade is made of six different material types, whose mechanical properties are summarized in Table 2. Non-structural masses are accounted for with both span-wise and chord-wise proportional quantities. A first estimate of the secondary design parameters, represented by the skin core thickness, is obtained using the preliminary design formulas described in §3.4.

Table 1 Structural configuration

Component	Starting section (% span)	Ending section (% span)	Material type
Skin	0	100	Stitched triaxial -45/0/+45 fiberglass
Spar caps	3	97.8	Unidirectional fiberglass
Shear webs	10	97.8	Stitched biaxial -45/+45 fiberglass
Trailing and leading edge reinforcements	10	80	Unidirectional fiberglass
Skin core	10	97.8	T500 Foam
Web core	10	97.8	T400 Foam

Table 2 Material properties

Material type	Longitudinal Young's modulus [MPa]	Transversal Young's modulus [MPa]	Shear modulus [MPa]
Stitched triaxial -45/0/+45 fiberglass	28500	10300	6400
Unidirectional fiberglass	38200	8600	3500
Stitched biaxial -45/+45 fiberglass	9700	9700	10900
T500 foam	93	93	40
T400 foam	65	65	28

The coarse minimum weight structural sizing is based on DLCs 1.2, 1.4, 1.5, 1.6, 1.7, 2.2, 2.3 and 6.1 [2]. The design constraints include: placement of the first and second blade natural frequencies with at least 12% and 20% gaps respectively with respect to the three-per-rev harmonic, a maximum blade tip deflection of $\delta_{\text{tip}_{\text{adm}}} = 5$ m, max/min allowable stresses/strains and fatigue constraints (see Eq. (5)).

The frequency placement and max tip deflection constraints are active at convergence, and thus the design is driven by the blade flap bending stiffness. In addition, fatigue constraints are active in the skin between 10% and 40% span, where the largest chords occur, while constraints associated with stresses/strains are far from their respective limits. For this reason, static analyses performed at the fine level are limited to the loading condition that results in the maximum tip deflection.

Two different 3D models are generated using either mid-thickness shell elements or solid elements. For the shell model, the blade is discretized by isoparametric linear triangu-

lar and quadrilateral elements with layered composite properties. The solid model is based on isoparametric linear prismatic and hexahedral solid elements. For both models, the characteristic element side lengths are about 5 cm. All loads are applied to the spar caps using `RBE3` elements.

At first, possible differences between the coarse-level model and the detailed 3D models are investigated by performing modal, static, fatigue and buckling analyses. Next, bounds are updated for the constraints that fail verification, and the effects of loop closure on a subsequent coarse-level iteration are illustrated.

4.2 First multi-level iteration

4.2.1 Modal analysis

Table 3 reports the first flap-wise and edge-wise blade natural frequencies obtained with the 3D mid-thickness shell, 3D solid and beam `Cp-Lambda/ANBA` models. The associated vibration modes are visualized in Fig. 11.

Table 3 Comparison of the two lowest blade natural frequencies

	Shell	Solid	`Cp-Lambda/ANBA`
$\omega_{1,\text{flap}}$ [Hz]	0.8552	0.8533	0.8568
$\omega_{1,\text{edge}}$ [Hz]	1.0120	1.0076	1.0560

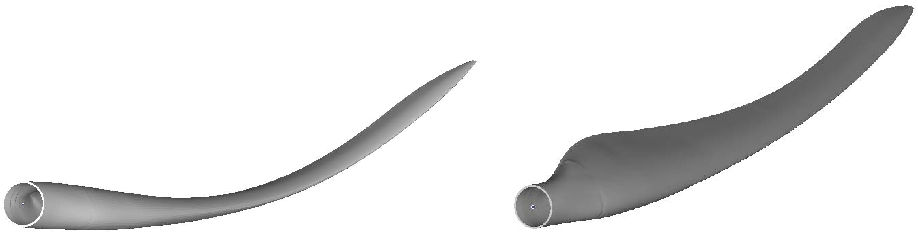

(a) First flap-wise vibration mode (b) First edge-wise vibration mode

Figure 11 The two lowest blade vibration modes

It is noted that the first flap-wise natural frequency agrees well for all models. On the other hand, the matching is not as good for the edge-wise mode, since the frequency predicted by the beam model is about 4% higher than the 3D ones. In the coarse-level optimization, this frequency is constrained to have a 20% margin with respect to the three-per-rev harmonic, and the constraint is active at convergence. To account for this, the constraint bound for this frequency is increased by 4% for the next coarse-level design iteration.

4.2.2 Static analysis

A static analysis for the load case corresponding to the maximum blade deflection is conducted next. A comparison of the flap- and edge-wise blade deflections obtained with the beam and 3D FE models reveals that all agree very well within a 0.02% margin.

On the other hand, as expected, the stress distribution shows much larger differences. Figure 12(a) and 12(b) plot the span-wise distribution of maximum stresses in the fiber direction of skin and caps, respectively.

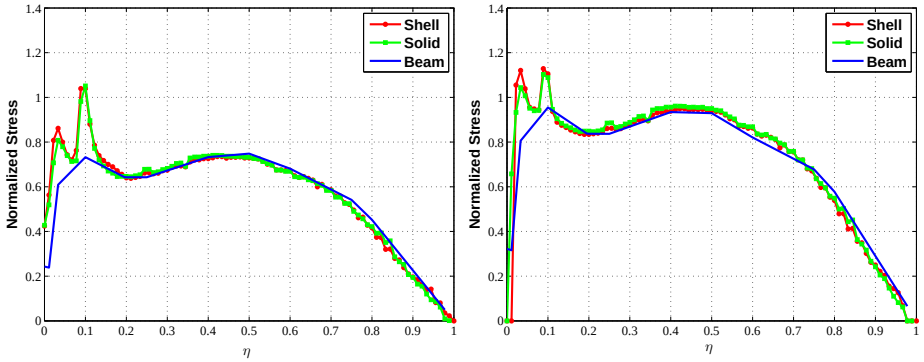

(a) Maximum skin stress (b) Maximum stress in spar caps

Figure 12 Normalized maximum stresses in the fiber direction

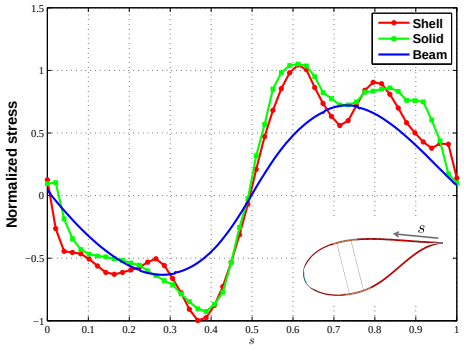

Figure 13 Normalized stress in the skin at the span-wise station $\eta = 0.10$, vs. curvilinear coordinate s

Figure 13 shows the skin-wise distribution of the longitudinal stress at 10% of blade span, plotted as a function of the non dimensional coordinate $0 \leq s \leq 1$. The importance of 3D effects in this blade region is particularly clear if one looks at the shell and solid models stress distributions and compares them to the beam one.

Significant relative differences are apparent at the root region, and in particular at the beginning of webs, leading and trailing edge reinforcements. The cause for these discrepancies is due to the simultaneous presence of rapid transitions in the local geometry and a

low skin thickness. The latter exhibits a rapid variation in the first 10% span, becoming only $1/20$ of the root thickness. The figures show that peaks arise exactly at the boundary region of the spar caps and the transition of the skin core, a complex region illustrated in Fig. 14.

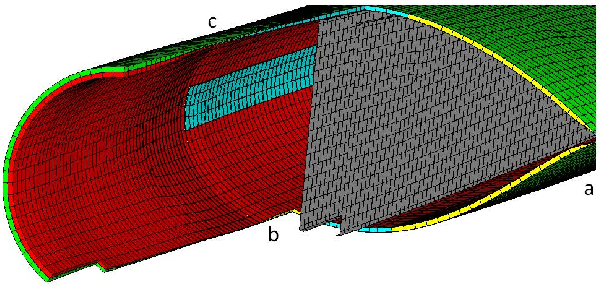

Figure 14 Detail of the blade root: a) trailing edge transition, b) beginning of skin core, c) beginning of spar caps

In summary, the investigation of static loading conditions clearly illustrates the need for a detailed 3D FE analysis in order to obtain reliable estimates of the stress field over the whole blade. While a beam model in general provides reasonable results for most of the blade span, it is however unable to describe the detailed stress field at critical three dimensional and rapidly varying regions.

4.2.3 Fatigue analysis

A fatigue analysis as described in §3.4 is performed using the mid-thickness shell model. Results for the fatigue damage index evaluated according to the multi-axial criterion of Eq. (6) at selected span-wise sections are illustrated in Fig. 15(a), along with comparable results obtained on the beam model.

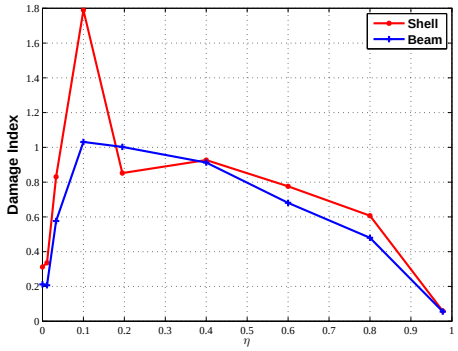

(a) Damage index vs. blade span

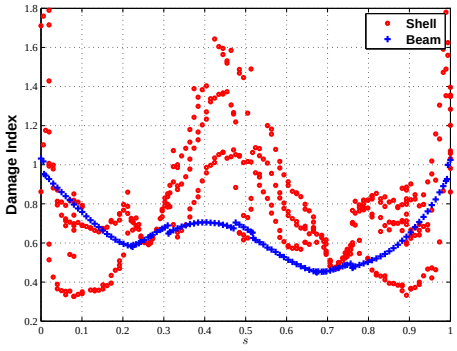

(b) Damage index at $\eta = 0.10$ span section, vs. curvilinear coordinate s

Figure 15 Damage index at selected verification points

It appears that the detailed 3D mid-thickness shell model predicts a significant peak at 10% span, violating the fatigue constraint. Similarly to the static analysis case, the peak is grossly underestimated by the coarse-level beam model.

Figure 15(b) plots the fatigue damage parameter in the skin at the most critical region, within a margin of 100 mm around 10% span. Fatigue damage is computed at points distributed along the airfoil, and plotted as a function of the curvilinear coordinate s. Similarly to the span-wise results, the 3D FE model predicts higher damage coefficients than the beam model, while both indicate the trailing edge region ($s = 0$ and $s = 1$) of the blade as the most exposed to fatigue.

4.2.4 Linear buckling analysis

Finally, a linearized buckling analysis of the 3D FE model is conducted by subjecting the blade to the loading condition of maximum tip displacement.

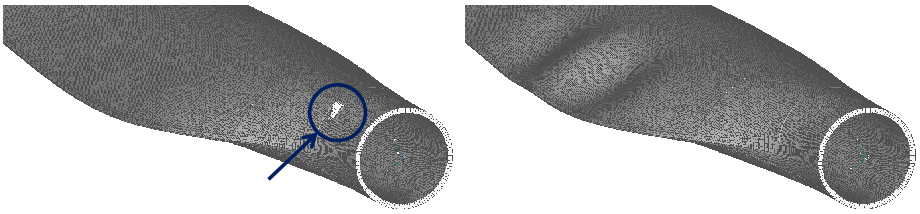

(a) First buckling mode, $\lambda_{\text{Shell}} = \lambda_{\text{Solid}} = 0.8$

(b) Second buckling mode, $\lambda_{\text{Shell}} = 3.594$, $\lambda_{\text{Solid}} = 3.4078$

Figure 16 Close-up view of first two buckling modes

The first two buckling modes are shown in Fig. 16(a) and 16(b). The first mode is localized near the blade root, while the second at the maximum chord region. Only the first mode is critical for the applied loading condition ($\lambda \leq 1$), and the instability is caused by the high compressive stresses that are generated around 10% span.

To correct for this, the structural capacity at this region would need to be increased. This can be done by using procedure (8), which would increase the skin core thickness. However, it should be noted that the same region of the blade failed the verification of the fatigue constraints. The update of the associated constraint bounds will induce, at the next coarse-level optimization, a modification of the primary structural parameters that will also induce a local strengthening of the structure. As a side effect, this might results in a sufficient buckling resistance for the original core thickness. In light of this observation, it was decided to avoid the update of the secondary design parameters, and wait for the result of the next coarse design iteration.

4.3 Closure of multi-level optimization loop

The closure of the loop between the coarse-fine analyses and back is illustrated by performing a second iteration. After the first iteration, the fine-level FE results identified the following critical aspects:

– The natural frequency spacing constraint is violated, as the 3D model edge-wise frequency is approximately 4% lower than the one predicted by the coarse-level beam model.
– Significant stress concentrations are present at the initiation sections of spar caps, shear webs and trailing and leading edge reinforcements, around 3% and 10% span.
– Fatigue constraints are violated at 10% span due to the same stress concentrations, with a fatigue damage index exceeding 1.8.
– The thickness of the blade skin core around 10% span is not sufficient to resist local buckling.

These results are used for tightening some of the constraint conditions for the next coarse iteration, which become:

$$\omega_{1,\text{edge}} \geq 1.04 \cdot 1.20 \cdot 3P, \tag{18a}$$

$$d(\boldsymbol{p}_s, D)_{10\%\ \text{skin}} \leq 1/1.8. \tag{18b}$$

The first condition modifies the edge-wise frequency spacing constraint, while the second corrects the fatigue condition at 10% span. Since stress peaks do not exceed allowables, no specific action is taken. For buckling, no action is taken to see if the strengthening induced by the tighter fatigue constraint is capable of fixing the problem.

The geometrical changes caused by the updated constraints are illustrated in Fig. 17(a) and 17(b).

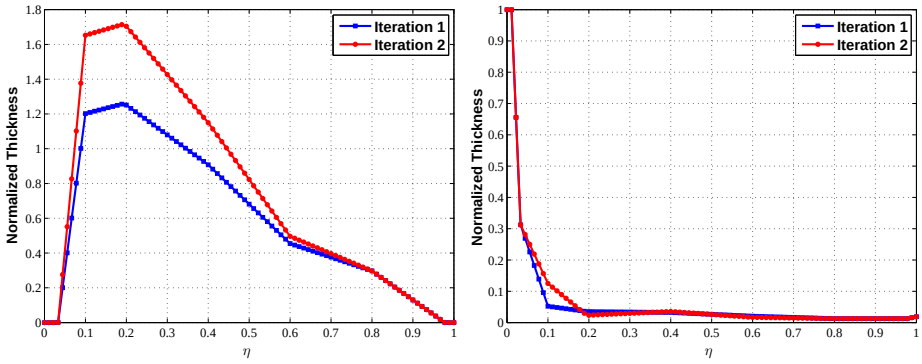

(a) Trailing edge reinforcement (b) Skin thickness

Figure 17 Normalized thicknesses of blade components

The trailing edge reinforcement has been significantly increased. This change is driven by the need for an increased edge-wise bending stiffness, required for the satisfaction of the modified frequency constraint condition, and the fine 3D edge-wise frequency now satisfies the 20% margin with the three-per-rev harmonic.

The skin thickness in the critical region at 10% span has been increased from 5% to 10% of the root thickness, so as to satisfy the more stringent fatigue constraint condition. This has in turn increased the total blade mass by about 1.2%.

The direct effect of increased skin thickness on the fatigue damage index computed on the fine 3D model is illustrated in Fig. 18. The figure shows that the previous peak at

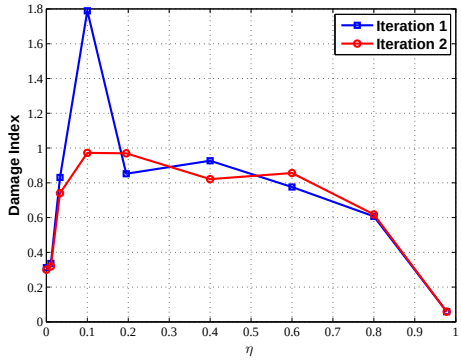

Figure 18 Damage index at selected sections along blade span

10% span is lowered to just below unity, indicating that the design now satisfies the fatigue requirement at the fine level.

Furthermore, as illustrated in Fig. 19(a), the previously identified skin stress concentrations are lowered in the critical region. In particular, the skin thickness increase at 10% span eliminates the stress peak at that same location, whereas the peak at 3% span, i.e. at the beginning of the spar caps, is only slightly reduced. Changes in the skin geometry affect also the spar cap stresses, which are similarly lowered as illustrated in Fig. 19(b).

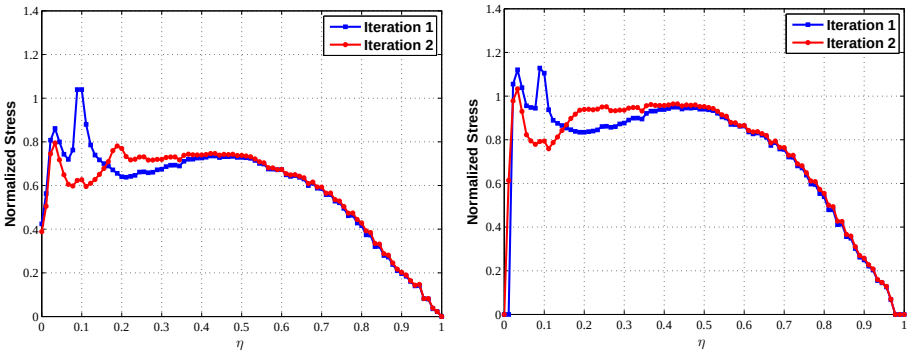

(a) Maximum stress $\sigma_{1,\max}$ in skin (b) Maximum stress $\sigma_{1,\max}$ in spar caps

Figure 19 Normalized maximum stresses in fiber direction

Finally, the increased skin thickness has an indirect effect on the buckling capacity. In fact the lowest buckling eigenvalue is now increased from 0.8 to 2.08, implying that the improved design exhibits sufficient buckling strength so that, in this particular case, a skin core thickness increase by the secondary design loop proves not to be necessary.

5 Conclusions

In this paper we have presented a multi-level optimization method for wind turbine rotor blades, that operates at different description levels to generate a cost-minimizing solution satisfying a number of design requirements expressed as inequality constraints.

The highlights of the proposed approach can be summarized as follows:

- Determination of the complete load envelope, including fatigue loads, by multibody aero-servo-elastic simulations conducted according to certification guidelines.
- Multi-disciplinary optimization by iteration between a multibody model and cross sectional 2D models, which provide the synthesis of fully populated stiffness matrices and the computation of sectional stresses and strains.
- Automatic generation of detailed 3D NURBS-based CAD model, accounting for all principal structural components, using either shell (with or without offsets) or solid descriptions.
- Automatic meshing of the models, including association of properties for anisotropic composite layered materials and loading conditions from the multibody aero-servo-elastic analyses.
- Complete re-analysis of the blade at the fine 3D FE description level, and verification of the satisfaction of the design constraints, including buckling.
- Heuristic update of the design constraints, based on the results of the fine-level re-analysis, and loop closure that enables successive coarse-level iterations until convergence.

The procedure was demonstrated on a 2MW wind turbine. After a first coarse-level optimization, detailed stress and fatigue analyses conducted on the fine-level 3D model revealed significant stress concentrations between the root and the maximum chord regions. These effects were not captured by the coarse-level beam model, which is blind to highly three-dimensional variations and abrupt changes in the stress field. Furthermore, the modal analysis of the 3D model showed the violation of a frequency constraint condition, while the buckling analysis highlighted the presence of skin instability under the maximum tip deflection loading condition. By tightening the respective constraint bounds for the subsequent coarse-level iteration, it was shown that convergence can be obtained very rapidly by iterating between the coarse and fine levels.

Although the skills of an experienced analyst is irreplaceable when conducting the design of complex engineering systems such as a wind turbine blade, the proposed highly automated design tools are believed to be able to streamline the design process and help in the exploration of the design space, relieving the burden of the most complex and error-prone tasks and allowing the user to focus on the understanding of the various design tradeoffs to come to the best possible solution.

References

1. Bottasso C.L., Campagnolo F., Croce A., Tibaldi C.: Optimization-based study of bend-twist coupled rotor blades for passive and integrated passive/active load alleviation. Wind Energy doi:10.1002/we.1543 (2012)
2. Wind Turbines — Part 1: Design Requirements, Ed. 3. International Standard IEC 61400-1 (2005)
3. Guideline for the Certification of Wind Turbines, Ed. 2010. Germanischer Lloyd Industrial Services GmbH, Renewables Certification, Brooktorkai 10, 20457 Hamburg, Germany (2010)
4. Lee D., Hodges D.H., Patil M.J.: Multi-flexible-body dynamic analysis of horizontal axis wind turbines. Wind Energy **5**, 281–300 (2002)

5. Bauchau O.A., Bottasso C.L., Nikishkov Y.G.: Modeling rotorcraft dynamics with finite element multibody procedures. Math. Comput. Model. **33**, 1113–1137 (2001)
6. Bottasso C.L., Croce A.: `Cp-Lambda`: User's Manual. Dipartimento di Ingegneria Aerospaziale, Politecnico di Milano (2006–2013)
7. Larsen T.J., Hansen A.M.: How 2 `HAWC2`, the User's Manual. Risø Report Risø-R-1597(ver. 3-1)(EN), Risø National Laboratory, Roskilde, Denmark (2007)
8. Jonkman J.M., Buhl Jr M.L.: `FAST` User's Guide. Technical Report NREL/EL-500-38230, National Renewable Energy Laboratory, Colorado, USA (2005)
9. `Bladed`. GL Garrad Hassan, St. Vincent's Works, Silverthorne Lane, Bristol, UK, www.gl-garradhassan.com
10. `RotorOpt` perfects rotor design. LM Glasfiber, News Letter, September, p. 5 (2007)
11. Fuglsang L.: Integrated design of turbine rotors. In: European Wind Energy Conference & Exhibition EWEC 2008, Brussels, Belgium, 31 March – 3 April (2008)
12. Duineveld N.P.: Structure and possibilities of the `FOCUS` design package. Dutch Wind Workshops, TU Delft, Delft, the Netherlands (2008)
13. Jonkman J.: NREL structural and aeroelastic codes. In: 2008 Wind Turbine Workshop, Sandia National Laboratories, Albuquerque, NM, USA, 12–14 May (2008)
14. Bottasso C.L., Campagnolo F, Croce A.: Multi-disciplinary constrained optimization of wind turbines. Multibody Syst. Dyn. DOI 10.1007/s11044-011-9271-x (2011)
15. Laird D.L.: `NUMAD` User's Manual - Numerical Manufactoring and Design Tool. Sandia Report SAND2001-2375, Wind Energy Technology, Sandia National Laboratories (2001)
16. Hoyt D.M., Graesser D.: Rapid FEA of Wind Turbine Blades — Summary of NSE Composites' structural analysis capabilities for blade NSE `bladeMesher` in-house software. NSE Composites, 1101 North Northlake Way, Suite 4, Seattle, WA 98103, May (2008)
17. Ashwill T.: Sweep-Twist Adaptive Rotor Blade: Final Project Report. Sandia Report SAND2009-8037, Sandia National Laboratories, Albuquerque, NM, USA (2010)
18. Jureczko M., Pawlak M., Mężyk A.: Optimisation of wind turbine blades. J. Mater. Process. Tech. **167**, 463–471 (2005)
19. Bauchau O.A.: Flexible Multibody Dynamics. Springer, Solid Mechanics and its Applications, Vol. 176 (2011)
20. Bauchau O.A., Bottasso C.L., Trainelli L.: Robust integration schemes for flexible multibody systems. Comput. Meth. Appl. Mech. Eng. **192**, 395–420 (2003)
21. Giavotto V., Borri M., Mantegazza P., Ghiringhelli G.: Anisotropic beam theory and applications. Comput. Struct. **16**, 403–413 (1983)
22. Bottasso C.L., Croce A., Nam Y., Riboldi C.E.D.: Power curve tracking in the presence of a tip speed constraint. Renew. Energy. **40**, 1–12 (2012)
23. `Matlab`. The MathWorks Inc., 3 Apple Hill Drive, Natick, MA 01760-2098, USA, www.mathworks.com
24. `HyperMesh`. Altair Engineering, 1820 Big River Rd, Troy, MI 48082, USA, www.altair.com
25. Philippidis T.P., Vassilopoulos A.P.: Complex stress state effect on fatigue life of GRP laminates. Part I, experimental. Int. J. Fatigue. **24**, 813–823 (2002)
26. Philippidis T.P., Vassilopoulos A.P.: Complex stress state effect on fatigue life of GRP laminates. Part II, theoretical formulation. Int. J. Fatigue. **24**, 825–830 (2002)
27. `MD/MSC NASTRAN` 2010 Quick Reference Guide. MSC Software (2010)
28. Drela M., Youngren H., `Xfoil`, Subsonic Airfoil Development System, web.mit.edu/drela/Public/web/xfoil
29. `MD/MSC NASTRAN` 2011 Linear Static Analysis User's Guide. MSC Software (2011)
30. Laird D., Montoya F., Malcolm D.J.: Finite element modeling of wind turbine blades. In: Proceedings of AIAA/ASME Wind Energy Symposium, Reno, Nevada, USA, AIAA-2005-0.195, p. 9–17 (2005)
31. Berry D.: Design of 9-Meter Carbon-Fiberglass Prototype Blades: CX-100 and TX-100. Sandia Report SAND2007-0201, Sandia National Laboratories, Albuquerque, NM, USA (2007)
32. Resor B.: Integrated Design and Analysis at Sandia. 2010 Sandia Wind Turbine Blade Workshop, Sandia National Laboratories, Albuquerque, NM, USA (2010)
33. Federov V.A., Dimitrov N., Berggren C., Krenk S., Branner K., Berring P.: Investigation of structural behaviour due to bend-twist couplings in wind turbine blades. In: Proceedings of International Conference on Composite Materials ICCM-17, Edinburgh, Scotland, 27–31 July (2009)
34. Chen J., Hallett S., Wisnom M.R.: Modelling complex geometry using solid finite element meshes with correct composite material orientations. Comput. Struct. **88**, 602–609 (2010)
35. `MSC NASTRAN` Element Reference Manual. MSC Software (2010)
36. Piegl L., Tiller W.: The NURBS Book (Monographs and Visual Communications), Ed. 2. Springer-Verlag, New York (1996)

37. Lee E.T.Y.: Choosing nodes in parametric curve interpolation. Comput. Aid. Des. **21**, 363–370 (1989)
38. Bishop N.W.M., Sherratt F.: Finite Element Based Fatigue Calculations. National Agency for Finite Element Methods & Standards (NAFEMS), Great Britain (2000)
39. Sullins R.T., Smith G.W., Spier E.E.: Manual for Structural Stability Analysis of Sandwich Plates and Shells. NASA Contractor report NASA CR-1457, Washington DC, USA, December (1969)
40. `Femap`. Siemens PLM Software, 5800 Granite Parkway, Suite 600, Plano, TX 75024, USA, www.siemens.com/plm/femap
41. Lindenburg C., de Winkel G.D.: Buckling load prediction tools for rotor blades. ECN-C-05-103, (2005)
42. Bruhn E.F.: Analysis and Design of Flight Vehicle Structures, Ed. 2. Jacobs Pub. (1973)